Configuring hydrogen lancing to reduce carbon and nitrogen oxides emissions from coal-fired rotary kilns

Citation for the original published paper (version of record):
Colin, S., Triana de Las Heras, F., Normann, F. et al (2025). Configuring hydrogen lancing to reduce carbon and nitrogen oxides emissions from coal-fired
rotary kilns. International Journal of Hydrogen Energy, 120: 323-332.
http://dx.doi.org/10.1016/j.ijhydene.2025.03.322

International Journal of Hydrogen Energy 120 (2025) 323–332

Contents lists available at ScienceDirect

International Journal of Hydrogen Energy

journal homepage: www.elsevier.com/locate/he

Configuring hydrogen lancing to reduce carbon and nitrogen oxides emissions from coal-fired rotary kilns

Samuel Colin [a,b,*], Francisco Javier Triana de Las Heras [b], Fredrik Normann [a,b], Andreas Johansson [c], Johannes Fernberg [c], Alexey Sepman [c], Jonas Wennebro [c], Henrik Wiinikka [c,d]

[a] Division of Energy Technology, Chalmers University of Technology, 41296, Gothenburg, Sweden
[b] Luossavaara-Kiirunavaara Aktiebolag, Box 952, 97127, Luleå, Sweden
[c] RISE AB, 94128, Piteå, Sweden
[d] Division of Energy Engineering, Luleå University of Technology, 97187, Luleå, Sweden

ARTICLE INFO

Handling Editor: Dr M Mahdi Najafpour

Keywords:
Hydrogen
Decarbonation
Combustion
NO_x
Co-firing
Rotary kiln
Integrated burner
Lancing
Solid fuel
Gaseous fuel
Spectroscopy
Photograph and video analysis

ABSTRACT

Coal replacement with hydrogen is a strategy for reducing carbon emissions from high-temperature industrial processes. Hydrogen lancing is a direct way for introducing hydrogen to existing coal-fired kilns. This work investigates the effects of hydrogen lancing on nitrogen oxides (NO_x) emissions and ignition behaviour in a pilot-scale furnace that employs a 30 % coal replacement with hydrogen lancing. The investigation encompasses the impacts of lancing distance, angling, and velocity. Advanced measurement techniques, including spectrometry and monochromatic digital cameras, characterise the flame and assess emissions.

The results indicate that the 30 % coal replacement by hydrogen lancing enhances combustion and reduces the emissions of carbon monoxides (CO). The flame characteristics vary with the location of the hydrogen injection, generally becoming more-intense than during coal combustion. NO_x emissions during lancing are similar or up to double the emissions observed for pure coal combustion, depending on the lancing configuration. Increasing the distance between the hydrogen lance and coal burner increases NO_x emissions.

1. Introduction

This work extends our previous experimental investigation [1] of the co-firing of hydrogen and coal in a rotary kiln process by evaluating hydrogen lancing[1] as an alternative to a coal-hydrogen combi-burner. The motivations for using hydrogen are coal replacement and process electrification to reduce carbon dioxide (CO_2) emissions. The motivations for the 30 % coal replacement rate is to allow for process adaptation, ramp up of industrial infrastructures, and to align with the Year 2030 decarbonization milestones, see for example European Union Climate Target Plan and the Paris Agreement. It is critical that the process conserves the flame characteristics and limits the formation of nitrogen oxides (NO_x), as NO_x has serious impacts on environment [2]. Our previous work [1] demonstrates that co-firing a fuel mixture of 30 % hydrogen and 70 % coal enhances coal ignition and flame stability, as compared to the combustion of pure coal. In addition, this co-firing approach results in reduced NO_x emissions compared with the combustion of either pure coal or pure hydrogen. The motivations for hydrogen lancing are ease of implementation and risk minimisation, as the current coal burner is maintained and disruption of production is reduced.

Retrofitting a rotary kiln to use a new fuel faces two main challenges: the change in flame properties; and the emission of NO_x. It is crucial to preserve the flame properties, so as to ensure process stability and product quality. Research on the flame characteristics of hydrogen-coal co-firing are scarce. Few studies have focused on flame characterisation during the co-firing of hydrogen and coal [3–7], although these studies have been limited with respect to rotary kiln conditions. Furthermore,

* Corresponding author. Division of Energy Technology, Chalmers University of Technology, 41296, Gothenburg, Sweden.
E-mail addresses: samuel.colin@lkab.com, samuelco@chalmers.se (S. Colin).

[1] Lancing: This term refers to the introduction of fuel through a pipe without any primary airflow.

https://doi.org/10.1016/j.ijhydene.2025.03.322
Received 7 February 2025; Received in revised form 17 March 2025; Accepted 21 March 2025
Available online 26 March 2025

no studies have specifically investigated the impact of hydrogen injection location within a coal jet. Adding hydrogen to coal has been found to enhance the release of volatiles [3], due to the high heating rate and the temperature of the coal particles. Although the char combustion rate may decrease due to the reduced availability of oxygen in the char combustion zone [4], hydrogen addition has been shown to enhance the combustion of pulverised coal [5]. Hercog et al. have indicated that co-firing high shares of alternative fuels in a rotary kiln for cement production is possible without any negative effect on combustion performance [8]. In line with this, in our previous work [9], we have shown that the characteristics of a solid fuel flame are ensured already at low levels of particle introduction to a gaseous flame. However, this observation is based on research that involved propane and lignite combustion at a lower furnace temperature than that used in full-scale rotary kilns.

Two advanced measurements techniques are relevant for characterising the flame: spectrometry; and image analysis with a *charge-coupled device* (CCD) camera. Spectroscopy has emerged as a critical tool for analysing the temperature and element concentrations in a flame [10–12]. One of its strengths is that it is non-intrusive. Research has shown that spectral emissions from coal particles can be used to calculate their temperature [10,13,14]. Similarly, digital cameras offer the ability to study the visual characteristics of the flame in a non-intrusive and simple way. These characteristics include the intensity, shape, size, and homogeneity of the flame, and the acquired information can provide further insights into the combustion state [15–19].

The introduction of hydrogen also affects the combustion environment and NO_x formation. NO_x emissions from pulverised coal flames in rotary kilns are believed to originate mainly from the fuel-bound nitrogen, although thermal NO_x formation through the Zeldovich mechanism is also important [20–22]. For hydrogen flames, it is believed that the formation of NO_x in hydrogen flames is largely dominated by thermal NO_x [23–25]. Wiinika et al. [26] and Sepman et al. [27] have shown that under iron ore rotary kiln conditions, the levels of NO_x emissions are considerably higher during hydrogen firing than during firing with solid fuels such as coal or biomass. Co-firing solid and gaseous fuels, including mixtures of hydrogen and coal, may reduce NO_x emissions relative to single-fuel combustion [1,3,9,28]. However, there are also studies that have reported an increase in NO_x emissions when hydrogen is introduced to coal combustion [29,30] (note that these experiments were not performed for rotary kiln conditions).

This work investigates hydrogen lancing as a mean to replace up to 30 % of coal on an energy basis in rotary kiln heating. The following parameters are examined: the spacing between the coal burner and the hydrogen lance; the effect of angling the hydrogen lance towards the coal burner; and the velocity of the hydrogen. The performance is evaluated based on the flame characteristics and NO_x emissions in a 150-kWh, pilot-scale set-up.

2. Methods

2.1. Experimental furnace

Fig. 1 presents the experiments were performed in the 150-kWh horizontal industrial combustion kiln (HICK) at RISE in Piteå, Sweden. This furnace is configured to suit iron-ore rotary kiln conditions. A detailed description of the furnace and previous experimental campaigns can be found elsewhere [1,26].

Pulverised coal and hydrogen served as the primary fuels. Table 1 provides the coal particle size distribution, and Table 2 lists the results for the coal proximate, ultimate, and calorimetric analyses, together with references to the methodologies employed for the fuel analyses. The hydrogen has a purity of >99.9 vol-% H_2.

2.2. Burner and lancing configurations and test cases

In total, eight separate lancing configurations were tested and compared with a hydrogen-coal reference combi-burner, B_160_REF, which was previously used in the first study as is denoted as 'O-A' in Ref. [1]. The cases are summarised in Table 3. Three days of measurements were needed for testing all of the cases. In addition to the test cases, each experimental day started and ended with the running of a coal reference case that consisted of 100 % coal. The coal reference cases are designated as, for example, Coal_12, where the first number indicates the day (Day 1 in this case) and the second number indicates if it is the starting or ending reference ('2' refers to ending). Two principal lancing configurations are distinguished: H_2 lance-burner at a distance of 70 mm (L); and H_2 lance-burner at a distance of 30 mm (N). The lance-burner distance is measured from the centre of the coal pipe to the centre of the H_2 lance. The coal pipe diameter is 18 mm, and 70 mm and 30 mm correspond to 3.9-times and 1.7-times the coal pipe diameter, respectively. Hydrogen inlet velocities in the range of 140–1240 m/s were tested. In addition, hydrogen lances angled towards the coal

Table 1
Coal particle size distribution.

Particle size (μm)	(%)
<1	2.1
<5	15.6
<10	29.2
<15	39.5
<20	47.6
<45	71.7
<63	81.3
<90	89.8
<125	95.2
<180	98.5
<250	99.6

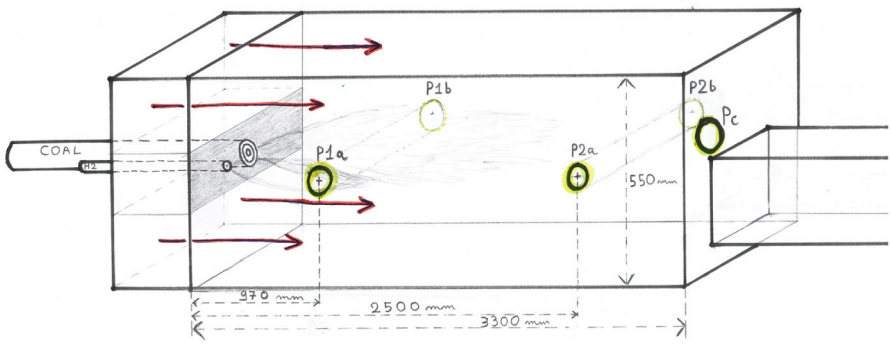

Fig. 1. Schematic of the horizontal industrial combustion kiln (HICK). The measurement ports are labelled as follows: P1a, P1b, P2a, and P2b are the optical ports for the spectrometric measurements; and Pc is the port for the CCD camera. Gas sampling is performed at the outlet of the furnace.

Table 2
Coal proximate, ultimate, and calorimetric analyses.

Proximate analysis (as-received)	Composition (%)	Standard
Moisture	0.5 ± 0.05	ISO 589:2018 mod
Volatile matter	19.2 ± 1	ISO 562:2010 mod
Fixed carbon[a]	68.2 ± 5	ISO 562:2010 mod[a]
Ash	12.1 ± 0.6	ISO 1171:2018
Ultimate analysis (as-received)	**Composition (%)**	**Standard**
Cl	<0.01	ASTM D4208-2019 mod
S	0.3	ASTM D4239-2018
C	77.0	ASTM-D5373:2016
H	3.9	ASTM-D5373:2016
N	1.33	ASTM-D5373:2016
O[a]	5.3	ASTM D3176-2015[a]
alorimetric analysis (as-received)	**Specific energy (MJ/kg)**	**Standard**
LHV	30.473	ISO 1928:2020

[a] Denotes calculated values.

burner at 15° (V), and pushed inside the furnace to a depth of 100 mm (I) were tested.

Table 4 depicts the nozzles and flows of the coal burner reference, the combi-burner reference, and the lancing configurations. In the B_160_REF combi-burner, the coal was injected at the centre, while hydrogen was injected through eight holes that are symmetrically spaced around the coal flow. An outer air flow, referred to as the *primary air flow*, covered the hydrogen and coal flows. No swirl was set for the primary air flow. The distance between the hydrogen injection and the centre of the burner was approximately 16 mm. The reference coal flow was fixed at 15 kg/h with transport air at 200 lpm. For the co-firing cases, the coal flow was 10.5 kg/h with transport air of 150 lpm. In all cases, primary air was set without swirl at a flow rate of 400 lpm. The hydrogen lances were operated with a flow rate of 234 lpm, which corresponds to 39 kW, and without any air flow. The hydrogen lances were not cooled.

2.3. Measurements

The measurements performed during the experimental campaign entailed the acquisition of digital images with a monochrome CCD camera, coal particle temperatures calculated from the emission spectra measured with a spectrometer, and gas concentrations measured using the Testo 350 and MGA Prime Air gas analysers.

2.3.1. Digital images

The Allied Vision Prosilica GT1910 monochrome CCD camera was mounted in the furnace back-end (Port Pc in Fig. 1, to measure the area, intensity, and contrast level of the flames. The procedure is summarised in Fig. 2.

The flame was visualised in the opposite direction to the burner inlet. Videos were acquired at regular intervals at the operating points, at 25 frames per second with a resolution of 1920 × 1080 pixels. The aperture was F1.8 and the exposure times ranged from 80 μs to 500 μs. In order to compare the videos taken with different exposure times, the grey values were corrected to a reference exposure time of 200 μs. A linear behaviour between the intensity and the grey scale value given by the camera was assumed. Recordings that had more than 10 % of their frames saturated were excluded. In total, including the reference coal cases, 60 videos consisting of 800 frames each were successfully recorded (approximately six videos per case study). Saturated frames inside the accepted videos were ignored during the analysis.

Table 4
Illustration of the burner nozzles and specifications of the burner/lance flows. 1. Coal-flow, 2. Primary air flow, and 3. Hydrogen flow.

100 % Coal	Co-firing - integrated burner B_160_REF	Co-firing – Lance burner
		
Black region: 15 kg/h coal +200 lpm transport air. Red region: Primary air – 400 lpm.	**Black region:** 10.5 kg/h coal +150 lpm transport air. Red region: Primary air – 400 lpm. Blue region: H_2 234 lpm (39 kW).	**Black region:** 10.5 kg/h coal +150 lpm transport air. Red region: Primary air – 400 lpm Blue region: H_2 234 lpm (39 kW).

Table 3
Summary of the lances and burners configurations evaluated during the experimental campaign. In the drawings, the black region marks the coal injection location, the red regions represent the primary air inlets, and the blue regions indicate the hydrogen gas injection points.

Co-firing configurations	Velocity (m/s)	CC[a]	Case nomenclature	Comments
B 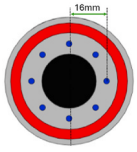	160	-	**B_160_REF**	Reference combi-burner
N 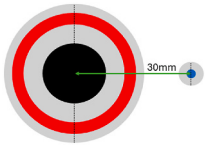	140	0.592	**N_140**	
			N_140_I	100 mm inside the furnace.
			N_140_V	At an angle of 15° to the coal flow.
	550	1.046	**N_550_V**	At an angle of 15° to the coal flow.
	1240	5.262	**N_1240**	
L 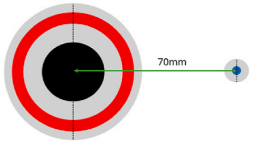	140	0.592	**L_140**	
			L_140_V	At an angle of 15° to the coal flow.
	1240	5.262	**L_1240**	

[a] CC corresponds to the Craya-Curtet number calculated using the same method as described in Ref.[31].

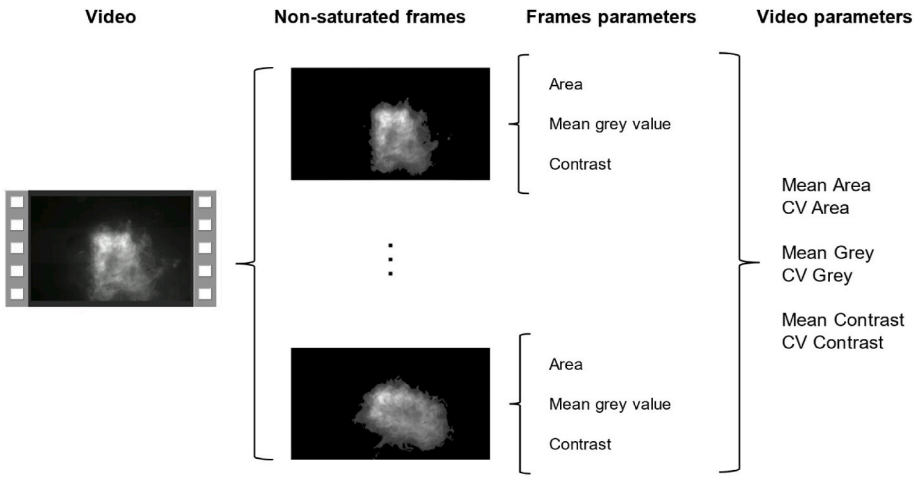

Fig. 2. Diagram summarising the procedure for treating the raw videos to extract the visual parameters.

The flame is identified in the image by applying intensity thresholding, i.e., a pixel with a value higher than a given threshold is considered part of the flame, otherwise it pertains to the background. However, it is not straightforward to define what a flame is. The task is even more challenging when different burners and exposure times are being analysed. In this work, the reference flame B_160_REF, recorded with an exposure time of 200 μs, was used to select a threshold of 55 by visual inspection. This was observed to be approximately the maximum grey value of the background. The resulting "flames" are illustrated in the second column of Fig. 2. The same intensity level was used for defining the flame in the other burners.

The image is characterised by two statistical measures: the mean; and the coefficient of variation. Their formal definitions can be found in Appendix A.1. The set of points $X = (x_1, x_2, \ldots, x_n)$ to which these statistical parameters are applied corresponds to the grey scale values of the pixels conforming the flame. Three visual features are calculated: area, intensity, and contrast. For a given frame, the area is defined as the number of pixels conforming the flame. In other words, it is the number of pixels with a grey value higher than the threshold value, or the number of points x_i. Then, the average intensity of the flame is represented by the mean grey scale value of the pixels inside the flame. Finally, the contrast of the flame is defined as the coefficient of variation of the grey values of these pixels.

For a given video, the area, intensity, and contrast of all its (non-saturated) frames are determined. Then, the mean value and coefficient of variation of each parameter are calculated. Overall, six parameters are assessed per video: the mean area (Mean Area); the coefficient of variation of the area (CV Area); the mean grey value (Mean Grey); the coefficient of variation of the grey value (CV Grey); the mean contrast (Mean Contrast); and the coefficient of variation of the contrast (CV Contrast).

2.3.2. Coal particle temperature and furnace temperature measurements

The spectrometer (Ocean Optics HR2000+GC) measured the emissions spectra from optical Ports P1 and P2 in both the a-side (being the side of the hydrogen injection) and b-side (termed P1a, P1b, P2a and P2b in Fig. 1). Three variables were extracted from the measurements: the particle temperature, the ignition zone, and the percentage of non-ignited particles.

The surface temperature (particle or furnace wall) was calculated using Planck's law in the measured wavelength range of 650–749 nm, to avoid strong interference from CO_2 and water. This method has been successfully applied and described in detail in previous works [10,27].

The ignition location may be estimated by calculating the coefficient of variation of the particles' temperature (CV Spectrometer). The definition of CV is found in the Appendix. As the radiation of the coal particles becomes insignificant at low temperature their contribution to the spectra becomes insignificant when not ignited. In this case the spectra is dominated by radiation from the opposite wall. The non-ignited particles are defined as the percentage of temperature measurements made by the spectrometer that are equal or lower than those for the opposite wall temperature with a margin of ±100 °C. A sensitivity analysis showed that changing the margin to ±0 °C or ±200 °C yielded equivalent results.

Besides the spectrometer, seven thermocouples (type K) were implemented to measure the operating temperatures. These thermocouples are mainly for operation and control and not for research as they provide indicative values of the oven's temperature. The thermocouples were cleaned of coating on a regular basis; however, they were not protected from coating.

2.3.3. Gas concentrations

The compositions of the flue gases were measured at the furnace outlet. The measured gas components included O_2, CO_2, CO, NO, and NO_2. The analyser was a Testo 350, which uses chemical cells to determine gas components (dry basis), with the exception of CO_2, for which an IR cell was utilised.

3. Results

This section presents the essential data obtained from the measurement devices, and the following section will discuss these results.

3.1. Visual parameters and temperature

Fig. 3 presents a representative image for each case study. The visual characteristics of the flame (area, intensity, shape, stability) varied significantly across the different configurations. The visual flame was attributable to the combustion of coal particles, as the hydrogen flame was not detectable with the camera settings used. A colour map was applied to represent visually the iso-levels of intensity.

The coal flames (first two rows in Fig. 3) were diffuse and unstable in appearance, having a low intensity in the visual spectrum, as compared with the co-firing cases. It is noteworthy that the coal references during Day 3 had higher intensity than during Days 1 and 2. Presumably, the furnace was warmer on the last day, thereby enhancing the coal combustion, as confirmed by the temperature measurements (see Fig. 4).

The reference coal-hydrogen combi-burner (B_160_REF) (lower-left corner of Fig. 3) displayed an intense, stable, and clearly defined flame. When the hydrogen lance was positioned near the coal burner (N_ cases), the visual flame became broader and more intense. Notably, the effect of increasing the velocity of the proximal burner appeared to thin the flame

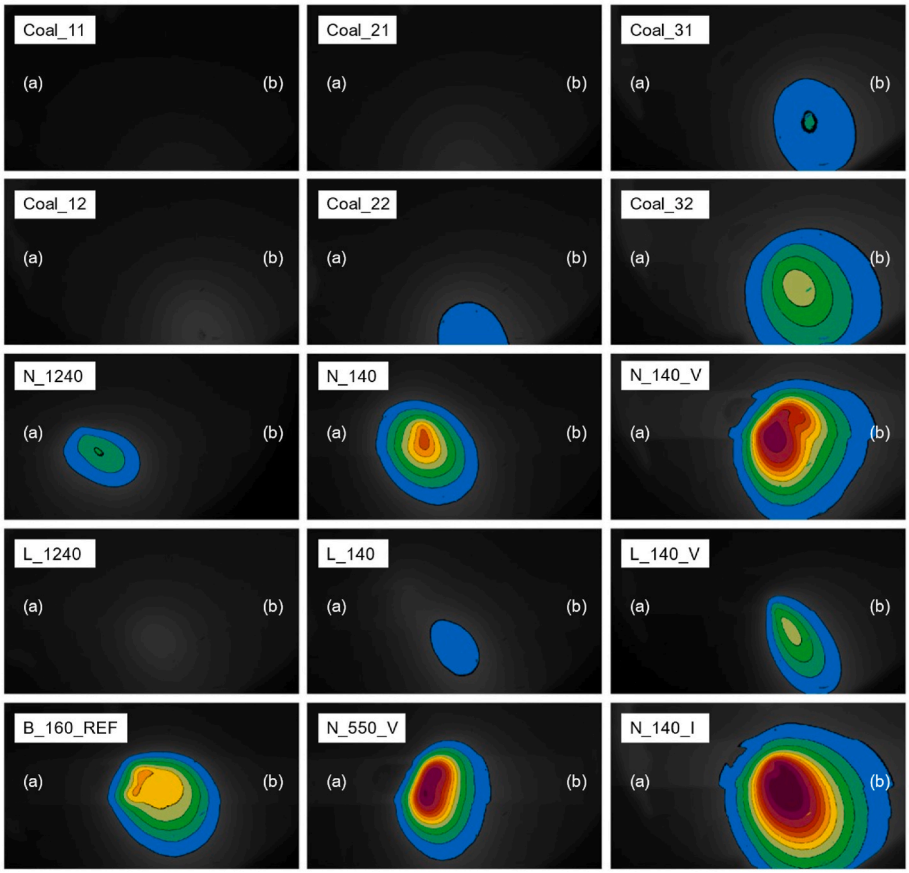

Fig. 3. Representative image for each burner configuration. The images are calculated using videos that have less than 10 % of their frames saturated. Furthermore, the saturated frames within those videos are ignored. Each column refers to 1 day of measurements, with the first two rows serving as the 100 % coal reference.

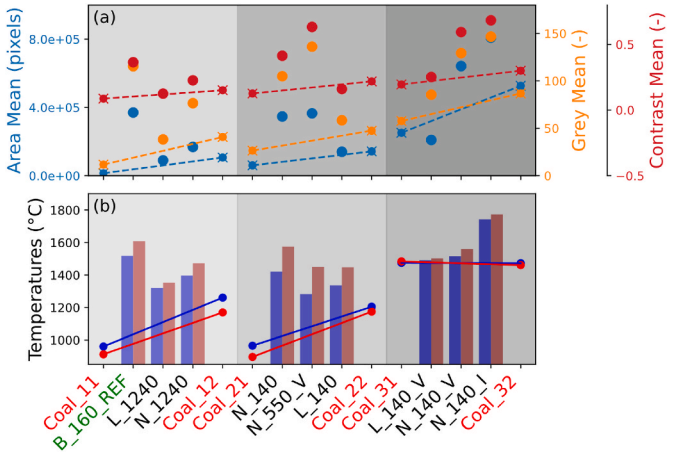

Fig. 4. Plot (a) presents the Mean Area, Mean Grey, Mean Contrast on the *y*-axis and plot (b) presents the average temperature in Port 1 for both the a-side (blue) and b-side (red) for the lancing configurations. For both plots, the *x*-axis corresponds to the cases in chronological order. For clarity, the *y*-axis scale in (b) starts at 850 °C. The coal reference is indicated in red font, and the combi-burner is in green font. The three shades of grey indicate Days 1–3. (For interpretation of the references to colour in this figure legend, the reader is referred to the Web version of this article.)

further and shift it upwards (see N_1240). For the configuration in which the H_2 lance was positioned farther from the coal burner (L_ cases), the visual flame resembled the coal reference more closely. Finally, the introduction of the hydrogen lance further into the furnace enlarged the flame (cf. N_140_I versus N_140).

The previous analysis can be summarised quantitatively according to the Mean Area, Mean Grey, and Mean Contrast. These parameters are shown for all cases in Fig. 4 (a). The values were obtained by averaging the visual parameters of all the videos associated with a burner configuration.

Not only did the visual features of the flame differ between the cases, but so did the temperature of the coal particles. Thus, to complement the visual parameters, the coal temperature measurements made at Ports P1a and P1b, based on averaging 200 spectra, are included in Fig. 4 (b). The coal reference is shaped by one line per day to evaluate the evolution of the conditions in the furnace during one day of trial.

Regarding the coal references, both Days 1 and 2 exhibit a significant temperature increase throughout the day. Day 3 shows a markedly higher temperature, which has clear impacts on the Mean Area and Mean Grey. Nevertheless, the Mean Contrast does not show any major changes.

The temperature of the coal particles for all the co-firing cases was higher in Port 1 and lower in Port 2, as compared with the coal cases. During the last day of the campaign, the increase in furnace temperature diminished the disparity between co-firing and coal cases. Yet, the Mean Grey and Mean Contrast showed higher values, reflecting a more-intense and defined flame for the co-firing cases. The combi-burner B_160_REF exhibited a higher temperature at Port 1 compared to lancing, except for Day 3 when the furnace conditions were different.

Concerning the lancing configurations, the temperature of the coal particles in Port 2 showed little fluctuation, except for the N_140_I case, which exhibited a significant temperature increase in both Ports 1 and 2. In Port 1, the differences between the cases were more prominent. Positioning the hydrogen lance closer to the coal burner increased the

coal particle temperature on both sides. Similarly, there was a notable increase in the Mean Grey, and a slight increase in the Mean Contrast. The Mean Area remained relatively constant. These observations were more pronounced for low velocities (L_140, N_140). All of the L_ cases had visual parameters similar to those of the coal cases.

Unfortunately, the angling of the hydrogen lance was difficult to evaluate because both L_140_V and N_140_V were run on Day 3, i.e., at higher temperature. Thus, they could not be directly compared to L_140 and N_140 but only relative to the coal reference. The lance-burner configuration with angling (L_140_V, N_140_V) induced only a slight increase in the coal particle temperature (of 40 °C) in P1. Visually, N_140_V showed a broader and brighter flame (high Mean Grey and Mean Contrast) than L_140_V, which presented with a remarkably low Mean Area.

The angled high-velocity case (N_550_V) displayed higher coal particle temperature differences between the a-side and b-side (~170 °C) than the low-velocity case (N_140_V) (~50 °C). While the furnace temperature may have impacted the difference, the camera observations showed that the angled high-velocity case, N_550_V, had a stronger flow hitting the coal particles than the low-velocity case, N_140_V. The visual parameters from the N_550_V indicated a high Mean Contrast and Mean Grey flame, although the flame was not particularly broad compared to the lower-velocity case.

Inserting the hydrogen lance 100 mm into the furnace with low velocity (N_140_I) increased the coal particle temperatures in both Ports 1 and 2, as compared with N_140. In Port 1, the temperature increases were 320 °C and 200 °C for the a-side and b-side, respectively. Even though the temperature differences were amplified by an overall higher furnace temperature during the last day, the temperature increase caused by the insertion of the lance was significant. The visuals for N_140_I showed the highest Mean Area, Mean Contrast, and Mean Grey of all the cases.

Overall, the co-firing cases exhibited higher temperatures at Port 1 compared to the coal reference. Furthermore, the co-firing flames were brighter and more stable/better defined, as demonstrated by the increased Mean Grey and Mean Contrast. The flame areas in the lance-burner configurations tended to be broader than in the coal reference. The general higher furnace temperature of the last day decreased the disparity between the furnace sides compared to Days 1 and 2, and the temperature showed less variation between the 100 % coal and co-firing cases.

3.2. Non-ignited particles and temperature variation

The percentages of non-ignited particles defined in the *Methods* section for each case studied are presented in Fig. 5 (a). Overall, the share of non-ignited particles in Port 1 was significantly higher with the use of pure coal than during co-firing. Nevertheless, significant differences were also observed between the lancing configurations. The nearest configuration, N_140, and the reference combi-burner, B_160_REF, did not exhibit any non-ignited particles. The N_550_V case impacted the ignition and coal particle temperature, and non-ignited particles were present on the a-side. Slightly less-pronounced, albeit notable effects, were observed in the L_140, N_1240, and L_140_V cases. Lastly, L_1240 showed a significant share of non-ignited particles on both sides, which resembled coal firing.

A final observation regarding the coal reference cases is that on Days 1 and 2 a higher proportion of non-ignited particles was observed on the b-side. This imbalance may be attributed to an asymmetrical temperature or secondary air flow distribution within the furnace. Nevertheless, data from the final day suggest that increased temperatures reduce this discrepancy or that the imbalance is not perceptible due to early ignition. These observations align with the findings from the image analysis.

Fig. 5 (b) relates the share of non-ignited particles to the coefficient of variation of the spectrometer (CV Spectrometer), which exhibits an inverse U-shaped pattern. The CV values were low (i.e. stable

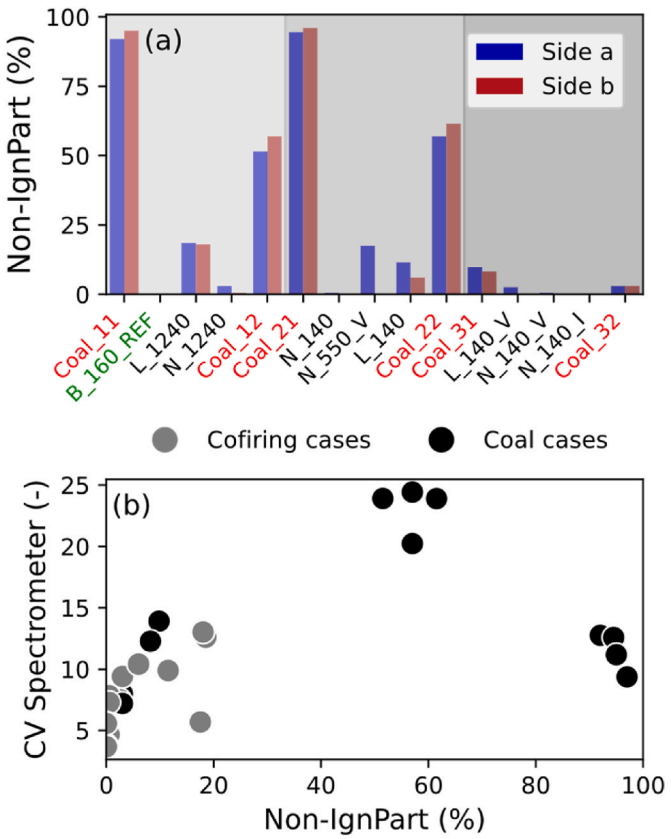

Fig. 5. (a) Percentages of non-ignited particles (Non-IgnPart) in each case study (parameter defined in the *Methods* section). The three shades of grey indicate Days 1–3. (b) Relationship between the non-ignited particles and the coefficient of variation of the spectrometer (CV Spectrometer). The grey data-points are the co-firing configurations, while the black data-points are the coal references. (For interpretation of the references to colour in this figure legend, the reader is referred to the Web version of this article.)

temperature measurements) when close to 0 or 100 % of the particles are non-ignited, but were high when the ignition zone is close to the measurement position, showing a peak in CV at around 50 % unignited particles. In Fig. 5 (b), the grey data-points are the co-firing configurations, while the black data-points are the coal references. For the co-firing cases, an increase in CV Spectrometer corresponds to an increase in non-ignited particles (0–20 %), that is the ignition is taking part later. Only the hydrogen side of the N_550_V does not follow this trend, likely caused by O_2 depletion. The oxygen depletion results from a strong local presence of H_2, due to the combination between the velocity and angle of the N_550_V.

3.3. Gas concentrations of O_2, CO and NO_x

The outlet O_2 concentration are relatively constant between all cases, although a slightly lower concentration is seen during coal-firing. Notably, the B_160_REF case exhibited significant variance in outlet oxygen concentration, due to instabilities in the coal feeding system during this case.

The later ignition and lower combustion efficiency during coal firing are reflected in higher outlet CO concentrations. The significantly reduced outlet CO concentration at the addition of hydrogen indicates an earlier ignition. The effect of hydrogen addition on CO emissions decreased during the last day when the furnace temperature was higher.

The measured NO_x outlet concentrations are presented in Fig. 6. NO_x is the sum of the measured NO and NO_2, expressed as mg NO_2/MJ_{fuel} to allow for comparisons across different furnace capacities.

Fig. 6 (b) presents the configurations ordered according to increasing NO_x emissions, with the red zone corresponding to the range of the coal reference fluctuating between 831 mg/MJ and 986 mg/MJ and a green line corresponding to the combi-burner reference B_160_REF that remained at the lowest value of 688 mg/MJ. The emissions doubled depending on the lancing configuration, varying from 846 mg/MJ in the N_550_V case to 1739 mg/MJ in the L_140 case. Increasing the distance between the coal and hydrogen lance or operating at 1240 m/s with the coal and hydrogen lance in close proximity resulted in a significant increase in the NO_x levels.

Angling the hydrogen lance at 15° to the coal flow decreased the NO_x emissions (−2.5 % and −32.0 % for the lance distances of 30 mm and 70 mm, respectively). When the hydrogen lance was set at 30 mm, an increase in velocity increased the level of NO_x by 28.4 %. At a lance depth of 70 mm, the level of NO_x decreased by 21.3 % with the same velocity increase.

3.4. Relationships between NO_x emissions and the visual parameters

Fig. 7 plots the NO_x emissions against the Mean Area (**a**), Mean Grey (**b**), and Mean Contrast (**c**).

For hydrogen lancing, higher average grey values, flame areas, and flame contrast values generally correlate with lower NO_x emissions. The Mean Area shows a weaker correlation than the Mean Grey and Mean Contrast values, with NO_x levels stabilising as the area increases further. An exception to this is when hydrogen is injected far from the coal (e.g., cases L_140 and L_1240). In case L_140, higher Mean Area, Mean Grey, and Mean Contrast are observed, yet the NO_x emissions are significantly higher. Overall, the findings suggest that a more-intense flame, with a clearly defined centre in the visible spectrum, tends to produce less NO_x. Notably, B_160_REF stands out with lower NO_x levels and reduced Mean Area, Mean Grey, and Mean Area compared to N_140_I, N_550_V, N_140_V, and N_140.

Fig. 8 shows the relationships between the levels of NO_x emissions and the CV Area (**a**), CV Grey (**b**) and CV Contrast (**c**). The CV of the visual parameters clearly correlates with the NO_x emissions: the higher the CV (instability), the higher the emissions. However, the correlation does not seem to hold for low instability (CV). For instance, cases N_140_I, N_550_V, and B_160_REF present a low CV Grey, although the NO_x emissions are significantly different.

The relationship between the point of ignition (indicated by CV Spectrometer) and the stability of the flame area (CV Area) is presented in Fig. 9 (a). A less-stable flame area tended to follow a later ignition. A similar trend was observed for the CV of the Contrast and Grey. The spectrometer measurements showed a more-robust response than the parameters extracted from the camera to observe variations as an indication of ignition.

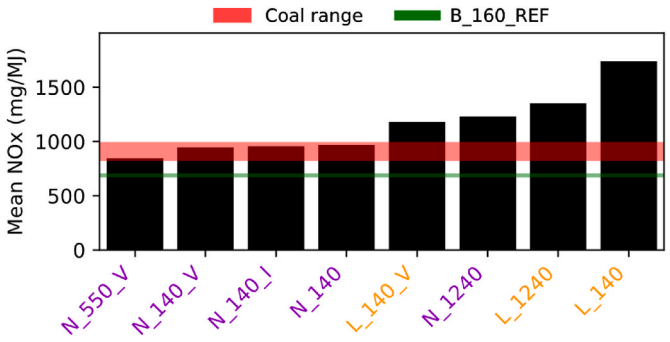

Fig. 6. NO_x emissions levels (in mg/MJ) ordered chronologically, with the coal reference range in red and the reference combi-burner in green. In plot (b), orange is used to represent the "L" cases, while purple represents the "N" cases. (For interpretation of the references to colour in this figure legend, the reader is referred to the Web version of this article.)

As shown by Fig. 9 (b), for the co-firing cases, later ignition was generally associated with higher NO_x emissions. In addition, the differences between the a-side and b-side of the CV Spectrometer diminished along with the increase in NO_x tending towards the behaviour of a 100 % coal flame. This is consistent with the previous measurements.

Fig. 9 (c) depicts the coal particle temperatures, using nuances of two colours to visualise the differences in the sides. The trend lines of the coal particle temperatures for both sides across all the cases remain nearly parallel regardless of the coal particle temperature, which decreases with increasing the CV of the spectrometer.

A caveat here is that correlation does not imply causation. Furthermore, measurements always entail some kind of constraint or limitation. It is essential to understand what exactly is being measured, and, consequently, the significance and robustness of the results. Thus, for instance, the digital images contain information that is only in the visible spectrum, and they were acquired from a specific position and with specific camera settings. When the hydrogen flame is placed far from the coal flame, the flame area, contrast, and grey value decrease. However, this might be due to the inability of the optical system to visualise the hydrogen flame.

In any case, correlations between the NO_x emissions, temperature stability, and visual parameters are clearly observed. While further experiments are essential to validate and fully understand these results, they indicate a potentially broader applicability of these observations.

4. Discussion

As indicated by the flame shape and visual parameters, hydrogen lancing significantly alters the flame's characteristics and emissions with non-uniform conditions surrounding the coal particles. First, the flame characteristics will be discussed, followed by a discussion of the nitrogen chemistry.

The image analysis and spectrometer measurements show that positioning the hydrogen lance close to the coal burner ("N_" configurations) enhances ignition and increases flame intensity, giving a more stable and distinct flame profile. This can be attributed to the interactions that occur between the fuels. Interactions where the hydrogen reacts faster than the coal, increasing the gas temperature and free radicals around the coal particles, favouring their ignition. The fast reaction may also disturb the flow turbulence and enhance the mixing of the hot secondary airflow with the coal stream. When the hydrogen lance is positioned closer to the coal, the velocity gradient increases, potentially promoting greater mixing with the surrounding air. This, in turn, may facilitate earlier ignition and accelerate the combustion process. The higher temperature of the coal particles increases their radiation intensity, which may promote a more-efficient coal combustion, particularly for char. The presence of water vapour may also accelerate char oxidation in the hydrogen side of the coal flame [3]. The enhancement of combustion by hydrogen lancing is supported by the decrease in outlet CO concentration, higher coal particle temperature in Port 1, and lower coal particle temperature in Port 2, as compared to coal firing. However, during high-velocity hydrogen lancing, the hydrogen jet may be shorter, which in turn may diminish the supportive effects to the coal flame initially seen at the lower velocity.

For configurations in which the hydrogen lance is located farther from the coal burner, the resulting coal flames are more diffuse, with lower density of reactions and, thus, lower intensity. Visually, these flames resemble the reference coal flame, and it is possible that the hydrogen and coal flames are completely separate. However, the L_140 and L_1240 cases show differences. The coal flame appears slightly brighter in the L_140 case. A low hydrogen velocity is believed to produce a larger flame compared to the higher velocities, potentially increasing the coal temperature through enhanced convective heat transfer, with a potentially modest contribution from increased radiation. Higher heat transfer from hydrogen to coal is reflected in the higher intensity observed in the image analyses and the reduced prevalence of

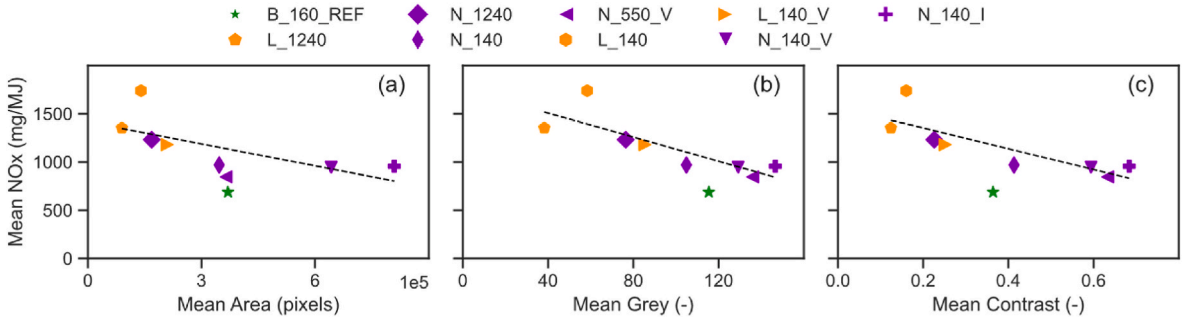

Fig. 7. Relationships between the levels of NO_x emissions and: a) Mean Area; b) Mean Grey; and c) Mean Contrast. Linear trend lines are added for support. Each shape represents a lance-burner configuration, with the combi-burner shown in green. No coal cases are present. The values for the visual parameters are derived from averaging the values from all the videos associated with a burner configuration. (For interpretation of the references to colour in this figure legend, the reader is referred to the Web version of this article.)

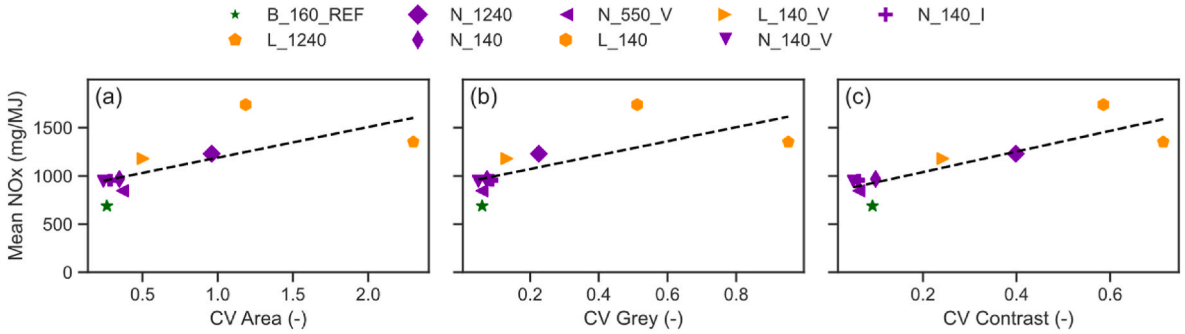

Fig. 8. Relationships between the levels of NO_x emissions and: a) CV Area; b) CV Grey; c) CV Contrast. Linear trend lines are added for support. Each shape represents a lance-burner configuration, with the combi-burner shown in green. No coal cases are present. The values for the visual parameters are derived from averaging the values from all the videos associated with a burner configuration. (For interpretation of the references to colour in this figure legend, the reader is referred to the Web version of this article.)

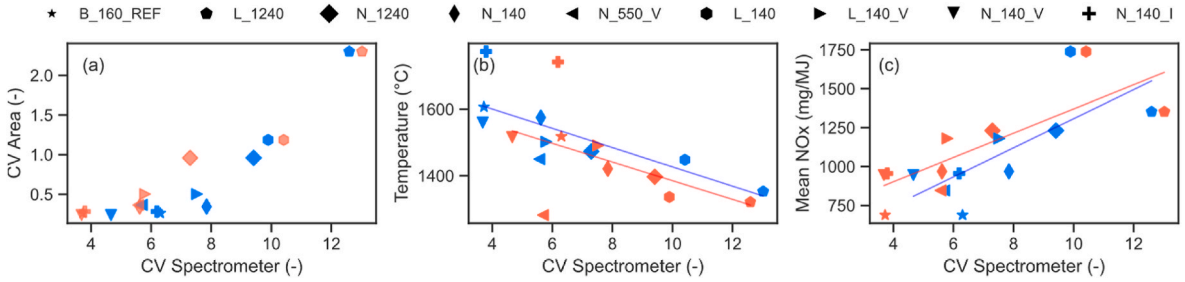

Fig. 9. (a) Coefficient of variation of the area as a function of CV Spectrometer for a-side and b-side; (b) Relationship between the temperature of the coal particles (y-axis) and their coefficient of variation (x-axis). (c) Relation between NOx emissions and the CV of the spectrometer. All the results shown are from Port 1. The blue and red colours correspond to the (a) and (b) sides respectively. (For interpretation of the references to colour in this figure legend, the reader is referred to the Web version of this article.)

non-ignited particles in the case of L_140. Angling the hydrogen lance increases the interactions and improves combustion performance, as the hydrogen is directed towards the coal flame, although the coal flame becomes more asymmetrical.

The cases with a visual high-intensity zone – within which the hydrogen interacts with coal particles – correlate with low NO_x emissions (N_550_V and N_140_V, as well as the combi-burner). In the reference coal-hydrogen combi-burner, the flame intensity diminishes in the bottom corner of the b-side, likely due to furnace turbulence events that cause the hydrogen to divert away from the coal in that region.

It is noteworthy that on the final day of the experiment, when the furnace operated at higher temperatures, the differences between the co-firing scenario and the 100 % coal combustion case were lower in comparison to those observed at lower temperatures. This suggests that the addition of hydrogen has a stronger impact on flame characteristics under poorer ignition conditions.

In terms of nitrogen chemistry, hydrogen influences three key factors associated with NOx formation. First, it alters reaction kinetics by modifying the distribution of inlet species and intermediate compounds. Although coal devolatilization produces hydrogen, it is negligible compared to a 30 % hydrogen co-firing scenario. Second, hydrogen affects local oxygen concentrations. Finally, it impacts the temperature distribution and overall flame temperature. The local temperatures of the coal particles appear to be higher in the presence of hydrogen, as evidenced by the intensities seen in the image analysis, and the level of O_2 might be lower as it is rapidly consumed by H_2. The combustion rate of coal particles does not increase as much on the a-side (hydrogen side) as on the b-side, which is attributed to a lower O_2 concentration around

the coal particles.

If the implementation of a hydrogen lance is not performed correctly, it is likely to trigger thermal NO_x formation. In those cases in which the hydrogen flame is separated from the coal flame (e.g., L_140 and L_1240), the gas volume at high temperature may be larger than during co-firing, increasing NO_x formation via the thermal NO_x route. In addition, local oxygen-to-fuel ratios are increased in the coal flow in separated flame configurations, inducing NO_x formation from the coal. In the case of L_140, the low velocity is believed to increase the volume of high-temperature gas in the hydrogen flame due to a longer flame, thereby promoting even more thermal NO_x. In contrast, when hydrogen penetrates the coal (N_cases), the conditions for NO_x reduction, such as re-burning effects, are favoured. Two main re-burning routes may be active: 1) the interaction between NO produced from Fuel-N (mostly HCN) and NH_3 or NH_2 generated by the presence of hydrogen at high temperature [32]; and 2) the interaction between NO and char combustion later in the flame [33]. The impact of char may be diminished by a higher concentration of H_2O, which can reduce the rate of heterogeneous char-NO reduction [34].

The reduced oxygen availability for coal combustion on the hydrogen side could help to lower the NO_x formation from both thermal NO_x and fuel-NO_x in the coal flame, creating a reducing zone in the coal flame. In conditions where hydrogen and coal are mixed, a part of the heat from the hydrogen flame is transferred to the coal particles, lowering the hydrogen flame temperature, and thereby decreasing the thermal NO_x. The enhancement of coal combustion by hydrogen may help, through an early ignition event, to decrease also the formation of NO_x [35]. Furthermore, data from both the Mean Grey measurements and the spectrometer indicate higher temperatures of the coal particles, which promote the release of Fuel-N in the volatiles rather than in the char. This change in partitioning is associated with lower NO_x emissions during coal combustion [36–40].

To deepen our understanding of NO_x chemistry under co-firing conditions, and to clarify the dominance of specific effects – particularly in asymmetrical flame configurations – additional experiments involving in-flame gas concentration measurements and modelling are required.

5. Conclusion

This study investigates the implementation of a hydrogen lance into a rotary kiln to replace 30 %-kW of the coal power and highlights the effects on and relationships between the combustion characteristics and NO_x formation.

The results indicate that the implementation of hydrogen lancing to coal combustion processes leads to a more-intense, concentrated, and stable flame. This is evidenced by the higher coal-particle temperatures observed in the early flame, which may be attributed to the high reactivity of hydrogen. The observation of asymmetrical temperature distribution, with lower temperatures on the hydrogen side, underscores the complex interactions that occur between coal and hydrogen during combustion. Reducing the distance between the coal and hydrogen lances increases the flame's area, intensity, and stability. Additionally, introducing a 15° angle to the hydrogen lance further amplifies the flame's area, intensity, and stability. This indicates that careful positioning of the hydrogen lance is crucial for maximising the benefits of hydrogen integration into the combustion process.

NO_x formation is highly sensitive to the configuration of the hydrogen lance. NO_x emissions increased by up to 100 % compared to coal combustion, and by as much as 250 % relative to the combi-burner reference. The reference combi-burner consistently gives the lowest NO_x emissions, and increasing the distance between the coal burner and hydrogen lance increases NO_x formation. The inlet velocity of hydrogen also affects NO_x formation: when the hydrogen lance is positioned at a distance of 30 mm an increase in velocity leads to a 28.4 % rise in NO_x emissions. In contrast, at a lance distance of 70 mm, the same increase in velocity results in a 21.3 % reduction in NO_x emissions. Implementation of the hydrogen lance at an angle of 15° to the coal flow reduces NO_x emissions by 2.5 % at 30 mm and by 32 % at 70 mm distance. To achieve the lowest NO_x emissions, we find that positioning the hydrogen lance as close as possible to the coal burner together with a low hydrogen velocity is optimal.

CRediT authorship contribution statement

Samuel Colin: Writing – review & editing, Writing – original draft, Visualization, Validation, Software, Methodology, Investigation, Formal analysis, Data curation, Conceptualization. **Francisco Javier Triana de Las Heras:** Writing – review & editing, Visualization, Methodology, Formal analysis, Data curation. **Fredrik Normann:** Writing – review & editing, Validation, Supervision, Resources, Project administration, Funding acquisition, Conceptualization. **Andreas Johansson:** Writing – review & editing, Investigation, Data curation. **Johannes Fernberg:** Writing – review & editing, Investigation, Data curation. **Alexey Sepman:** Writing – review & editing, Investigation, Data curation. **Jonas Wennebro:** Investigation, Data curation. **Henrik Wiinikka:** Writing – review & editing, Supervision, Investigation, Data curation.

Relevant results

- Implementation of a hydrogen lance improves the ignition and combustion processes.
- Relative to coal-only combustion, hydrogen addition can give up to double the level of NOx formation depending on the configuration of the hydrogen lance.
- Injecting the hydrogen close to the coal flow is in general favourable, with the hydrogen-integrated burner as the extreme, showing the lowest level of NO_x.
- A bright flame with a clearly defined centre (in the visible part of the spectrum) is shown to be beneficial in terms of reducing NO_x formation.
- A higher furnace temperature reduces the differences in flame characteristics between co-firing and 100 % coal combustion. However, the NO_x emissions levels differ significantly.

Declaration of competing interest

The authors declare that they have no known competing financial interests or personal relationships that could have appeared to influence the work reported in this paper.

Acknowledgements

Luossavaara-Kiirunavaara AB (LKAB). Swedish Energy Agency and the European Union (EU) are acknowledged for the financial support of this work (P2022-00196)

Appendix A. Supplementary data

Supplementary data to this article can be found online at https://doi.org/10.1016/j.ijhydene.2025.03.322.

References

[1] Johansson A, Fernberg J, Sepman A, Colin S, Wennebro J, Normann F, Wiinikka H. Cofiring of hydrogen and pulverized coal in rotary kilns using one integrated burner. Int J Hydrogen Energy 2024;90:342–52. https://doi.org/10.1016/j.ijhydene.2024.09.327.

[2] de Vries W. Impacts of nitrogen emissions on ecosystems and human health: a mini review. Curr. Opinion in Environ Sci Health 2021;21:100249. https://doi.org/10.1016/j.coesh.2021.100249.

[3] Xiao W, Cui J, Pan H, Zhao H, Yang S, Xue Z, Fu Y, Xu Y. A study on the influence of oxy-hydrogen gas flame on the combustion stability of coal powder and nitrogen

oxide emissions. Processes 2024;12(8):1777. https://doi.org/10.3390/pr12081777.
[4] Ueki Y, Yoshiie R, Naruse I, Matsuzaki S. Effect of hydrogen gas addition on combustion characteristics of pulverized coal. Fuel Process Technol 2017;161:289–94. https://doi.org/10.1016/j.fuproc.2017.02.034.
[5] Ren M, Liu W, Zhao J, Zou C, Ren L, Wu H, Zhao J. Effects of hydrogen fraction in Co-injection gas on combustion characteristics of the raceway in low carbon emission blast furnace. Int J Hydrogen Energy 2023;48(30):11530–40. https://doi.org/10.1016/j.ijhydene.2022.06.106.
[6] Wei D, Han S, Ji X, Wang T, Sun B. Numerical investigation of hydrogen Co-firing in a 660 MW power plants: combustion stability, heat transfer, and NOx formation. J Energy Inst 2024;113:101558. https://doi.org/10.1016/j.joei.2024.101558.
[7] Impacts of cofiring hydrogen in a coalfired steam boiler: numerical modeling assessment. https://www.epri.com/research/products/000000003002023986. [Accessed 20 December 2024].
[8] Hercog J, Lewtak R, Glot B, Jóźwiak P, Nehring G, Tavares VD, Nunes AM, Gaspar D. Pilot testing and numerical simulations of the multifuel burner for the cement kiln. Fuel 2023;342:127801. https://doi.org/10.1016/j.fuel.2023.127801.
[9] Colin S, Normann F, Fredriksson C, Andersson K. Flame characterization of cofiring gaseous and solid fuels in suspensions. ACS Omega 2024;9(26):28268–82. https://doi.org/10.1021/acsomega.4c01770.
[10] Wiinikka H, Sepman A, Ögren Y, Lindblom B, Nordin L-O. Combustion evaluation of renewable fuels for iron-ore pellet induration. Energy Fuels 2019;33(8):7819–29. https://doi.org/10.1021/acs.energyfuels.9b01356.
[11] Flame Spectroscopy, chapters: Atomic Emission Spectometry; The Alkali Metals; Luminescence| ScienceDirect Topics. https://www.sciencedirect.com/topics/chemistry/flame-spectroscopy (accessed 2024-August-21).
[12] Machado DA, Carinhana Junior D. *Determination of Flame Temperature by Emission and Absorption Spectroscopy*; Atena Edicão de Livros. PR: Ponta Grossa; 2024.
[13] Sun Y, Lou C, Zhou HA. Simple judgment method of gray property of flames based on spectral analysis and the two-color method for measurements of temperatures and emissivity. Proc Combust Inst 2011;33(1):735–41. https://doi.org/10.1016/j.proci.2010.07.042.
[14] Zeng Z, Zhang T, Zheng S, Wu W, Zhou Y. Ignition and combustion characteristics of coal particles under high-temperature and low-oxygen environments mimicking MILD oxy-coal combustion conditions. Fuel 2019;253:1104–13. https://doi.org/10.1016/j.fuel.2019.05.101.
[15] Lu G, Yan Y, Colechin M. A digital imaging based multifunctional flame monitoring system. IEEE Trans Instrum Meas 2004;53(4):1152–8. https://doi.org/10.1109/TIM.2004.830571.
[16] Sun D, Lu G, Zhou H, Yan Y. Flame stability monitoring and characterization through digital imaging and spectral analysis. Meas Sci Technol 2011;22(11):114007. https://doi.org/10.1088/0957-0233/22/11/114007.
[17] Sun D, Lu G, Zhou H, Yan Y, Liu S. Quantitative assessment of flame stability through image processing and spectral analysis. IEEE Trans Instrum Meas 2015;64(12):3323–33. https://doi.org/10.1109/TIM.2015.2444262.
[18] Moinul Hossain Md M, Lu G, Yan Y. Optical fiber imaging based tomographic reconstruction of burner flames. IEEE Trans Instrum Meas 2012;61(5):1417–25. https://doi.org/10.1109/TIM.2012.2186477.
[19] Hossain MM, Lu G, Sun D, Yan Y. Three-dimensional reconstruction of flame temperature and emissivity distribution using optical tomographic and two-colour pyrometric techniques. Meas Sci Technol 2013;24(7):074010. https://doi.org/10.1088/0957-0233/24/7/074010.
[20] Pershing DW, Wendt JOL. Pulverized coal combustion: the influence of flame temperature and coal composition on thermal and fuel NOx. Symposium (Int) on Combustion 1977;16(1):389–99. https://doi.org/10.1016/S0082-0784(77)80339-1.
[21] van der Lans RP, Glarborg P, Dam-Johansen K. Influence of process parameters on nitrogen oxide formation in pulverized coal burners. Prog Energy Combust Sci 1997;23(4):349–77. https://doi.org/10.1016/S0360-1285(97)00012-9.
[22] Edland R, Normann F, Fredriksson C, Andersson K. Implications of fuel choice and burner settings for combustion efficiency and NOx formation in PF-fired iron ore rotary kilns. Energy Fuels 2017;31(3):3253–61. https://doi.org/10.1021/acs.energyfuels.6b03205.
[23] Konnov AA, Colson G, De Ruyck J. NO formation rates for hydrogen combustion in stirred reactors. Fuel 2001;80(1):49–65. https://doi.org/10.1016/S0016-2361(00)00060-0.
[24] Zeldovich YB. In: Sunyaev RA, editor. 25. The oxidation of nitrogen in combustion and explosions. Princeton University Press; 1992. p. 364–403. https://doi.org/10.1515/9781400862979.364.
[25] Warnatz J, Maas U, Dibble RW. Combustion. Berlin, Heidelberg: Springer Berlin Heidelberg; 1996. https://doi.org/10.1007/978-3-642-97668-1.
[26] Wiinikka H, Sepman A, Ögren yngve, Lindblom B, Nordin L-O. Combustion evaluation of renewable fuels for iron-ore pellet induration. Energy Fuels 2019;33. https://doi.org/10.1021/acs.energyfuels.9b01356.
[27] Sepman A, Fredriksson C, Ögren Y, Wiinikka H. Laser-based, optical, and traditional diagnostics of NO and temperature in 400 kW pilot-scale furnace. Appl Sci 2021;11(15):7048. https://doi.org/10.3390/app11157048.
[28] Cui MS, Niu F, Ji RS, Duan L, Zhang X. Experimental study on flame chemical composition of coal and ammonia gas–solid jet in flat flame burner. ACS Omega 2024;9(10):11769–79. https://doi.org/10.1021/acsomega.3c09231.
[29] Pisa I, Lazaroiu G, Prisecaru T. Influence of hydrogen enriched gas injection upon polluting emissions from pulverized coal combustion. Int J Hydrogen Energy 2014;39(31):17702–9. https://doi.org/10.1016/j.ijhydene.2014.08.119.
[30] İlbaş M, Karyeyen S. A numerical study on combustion behaviours of hydrogen-enriched low calorific value coal gases. Int J Hydrogen Energy 2015;40(44):15218–26. https://doi.org/10.1016/j.ijhydene.2015.04.141.
[31] Larsson IAS, Johansson SPA, Lundström TS, Marjavaara BD. PIV/PLIF experiments of jet mixing in a model of a rotary kiln. Exp Fluid 2015;56(5):111. https://doi.org/10.1007/s00348-015-1984-9.
[32] Alzueta MU, Mercader VD, Giménez-López J, Bilbao R. NH3 oxidation and NO reduction by NH3 in N2/Ar and CO2 atmospheres. Fuel 2023;353:129212. https://doi.org/10.1016/j.fuel.2023.129212.
[33] Levy JM, Chan LK, Sarofim AF, Beér JM. NO/Char reactions at pulverized coal flame conditions. Symposium (Int) on Combustion 1981;18(1):111–20. https://doi.org/10.1016/S0082-0784(81)80016-1.
[34] Li Y, Sun R, Wu J, Wang Z, Wang M, Song Z. Effect of H2O on char-nitrogen conversion during char-O2/H2O combustion under high-temperature entrained flow conditions. Combust Flame 2019;207:391–405. https://doi.org/10.1016/j.combustflame.2019.06.013.
[35] Colin S, Normann F, Fredriksson C, Andersson K. Flame characterization of cofiring gaseous and solid fuels in suspensions. ACS Omega 2024;9(26):28268–82. https://doi.org/10.1021/acsomega.4c01770.
[36] Pohl JH, Sarofim AF. Devolatilization and oxidation of coal nitrogen. Symposium (Int) on Combustion 1977;16(1):491–501. https://doi.org/10.1016/S0082-0784(77)80346-9.
[37] Solomon PR, Colket MB. Evolution of fuel nitrogen in coal devolatilization. Fuel 1978;57(12):749–55. https://doi.org/10.1016/0016-2361(78)90133-3.
[38] Blair DW, Wendt JOL, Bartok W. Evolution of nitrogen and other species during controlled pyrolysis of coal. Symposium (Int) on Combustion 1977;16(1):475–89. https://doi.org/10.1016/S0082-0784(77)80345-7.
[39] Kambara S, Takarada T, Yamamoto Y, Kato K. Relation between functional forms of coal nitrogen and formation of nitrogen oxide (NOx) precursors during rapid pyrolysis. Energy Fuels 1993;7(6):1013–20. https://doi.org/10.1021/ef00042a045.
[40] Zhang H, Fletcher TH. Nitrogen transformations during secondary coal pyrolysis. Energy Fuels 2001;15(6):1512–22. https://doi.org/10.1021/ef010118g.